Liquid ammonia chemical lithiation: an approach for high energy and high voltage Si-graphite │ $Li_{1+x}Ni_{0.5}Mn_{1.5}O_4$ Li-ion batteries

Wesley M. Dose*[,1], James Blauwkamp[1], María José Piernas-Muñoz[1], Ira Bloom[1], Xue Rui[2], Robert F. Klie[2], Premkumar Senguttuvan[1], Christopher S. Johnson*[,1]

[1.] Chemical Sciences and Engineering Division, Argonne National Laboratory, Lemont, Illinois, U.S.A. 60439.
[2.] Department of Physics, University of Illinois at Chicago, 845 W Taylor Street, Chicago, Illinois, U.S.A. 60607.

*Correspondence: wdose@anl.gov, cjohnson@anl.gov

Abstract

Chemical lithiation using lithium metal dissolved in liquid ammonia is introduced for the first time as a viable, potentially scalable method to over-lithiate cathode materials, in this case, the 5V spinel $Li_{1+x}Ni_{0.5}Mn_{1.5}O_4$. In this formula the value of x represents the amount of extra lithium inserted into the spinel. Such over-lithiated cathodes can subsequently be used to pre-lithiate high–energy anodes in a lithium-ion battery configuration during the first charge step. Lithiated 5V spinel $Li_{1+x}Ni_{0.5}Mn_{1.5}O_4$ cathode materials prepared by this technique show higher first delithiation capacities, confirming the chemically inserted lithium is electrochemically active. Full cells with a Si-graphite anode and the $Li_{1+x}Ni_{0.5}Mn_{1.5}O_4$ (x=0.62) cathode show a 23 % higher reversible capacity in the first cycle than $LiNi_{0.5}Mn_{1.5}O_4$ baseline cells, and improved capacity retention. The extra, chemically inserted lithium therefore sacrificially compensates for the loss of lithium at the anode allowing higher utilization of the cathode capacity in following cycles.

Introduction

Lithium-ion batteries (LIB) are perhaps the most widely known energy storage device today. Their success in revolutionizing the mobile electronics market is now spreading to impact

upon the transportation and grid storage sectors.[1-2] While there are a number of cathode materials found in current commercial LIB, such as layered $LiCoO_2$ (LCO), $LiNi_xCo_yMn_{1-x-y}O_2$ (NCM), $LiNi_{0.8}Co_{0.15}Al_{0.05}O_2$ (NCA), olivine $LiFePO_4$ (LFP) and spinel $LiMn_2O_4$ (LMO), most use graphite as the anode. Graphite's enduring success since it was first commercialized by Sony in 1991 through to the present day is largely due to its respectable gravimetric capacity (372 mAh g^{-1}), low potential versus Li/Li^+, and long-term cycling stability. However, numerous next-generation anode candidate materials are currently being investigated which have much higher gravimetric capacities than graphite. For example, metal oxide conversion materials (e.g., MO where M is Co, Ni, Cu, Fe, Mn, Ru, etc.[3-4]) and alloy or conversion electrodes[5] such as silicon (3579 mAh g^{-1}),[6] tin (991 mAh g^{-1}),[7-8] germanium (1600 mAh g^{-1}),[9] and intermetallic compounds based on these.

Among these, silicon is currently considered one of the most promising future high energy anode materials. Several issues hamper the development of these electrode materials. The first is the large irreversible capacity (IC) in the first cycle, which is largely due to solid electrolyte interphase (SEI) formation[10-13] and other side reactions between the aprotic organic solvent in the electrolyte and the anode surface. While intercalation electrodes such as graphite have first cycle IC, it is limited to 8-10 % of the gravimetric capacity. In the case of Si, the large volume change during (de)lithiation expose fresh, unreacted surfaces that undergo further reactions, yielding an IC of ~27 % in the first cycle. Depending on the chemistry of the anode, this value can be as high as 40-50 %.[14-15] While not all IC is due to lithium ion consuming reactions, the majority of it is.[16] In a full cell, where the amount of available lithium is limited by that initially present in the cathode, the high first cycle capacity loss leads to a drastically lower energy density in subsequent cycles. A second equally problematic issue for Si anodes is the rapid capacity fade, which is also

primarily caused by losses of active lithium due to repeated particle expansion and contraction, passivation and re-passivation SEI reactions.[5, 17-19] Si particle degradation and electrode degradation are also accountable for the poor capacity retention.[19-22]

There are a growing number of strategies proposed to mitigate the first cycle IC of LIB anodes. These have been reviewed recently,[15] and include adding stabilized Li powder to anode materials, anode electrochemical lithiation, sacrificial lithium-containing salts on the cathode and anode, chemical lithiation of the cathode and anode, among others. In each of the above examples, a "lithium reserve" is added to the cell which, during normal cell operation and usually on the first cycle, is accessed. This releases available lithium to the cathode or anode that can be cycled, thereby adding lithium inventory to the cell. While these approaches have been shown to successfully account for the IC on the first cycle, addressing the ongoing active lithium losses on subsequent cycles is more challenging.[23]

In this work we introduce a new liquid ammonia-based chemical lithiation method as a means of introducing lithium reserve to the cathode. This synthesis technique is demonstrated for the high-voltage spinel cathode, $LiNi_{0.5}Mn_{1.5}O_4$ (LNMO). LNMO has generated considerable interest over the last decade due to its high energy density, high voltage, and excellent rate capability.[24] Also, this material is cobalt free, which is becoming ever more significant as the toxicity and high cost of cobalt are an increasing concern.[25] Important for this work, the LNMO spinel structure has unoccupied crystallographic sites that can accommodate lithium, a feature that has been capitalized upon in numerous previous reports.[26-29] In the last several years, there have been only a few reports where the over-lithiation capability of LNMO has been used to mitigate the IC. Manthiram et al.[14] employ a microwave assisted chemical lithiation technique using tetraethylene glycol as a reducing agent and $LiOH.H_2O$ as a lithium source. The resulting lithiated

LNMO, $Li_{1+x}Ni_{0.5}Mn_{1.5}O_4$ (LLNMO), is cycled versus FeSb-TiC and accounts well for the large IC of this anode. More recently, Wohlfahrt-Mehrens and coworkers[30-32] demonstrate synthesis of LLNMO by a coprecipitation process followed by two thermal treatment steps. To tailor the amount of lithium reserve in the cell the LLNMO is blended with un-treated LNMO and paired with graphite and silicon electrodes, compensating for the respectively small and large IC of both electrodes.[31] This work introduces for the first time a liquid ammonia-based chemical lithiation synthesis for over-lithiation of LIB cathodes. The LLNMO synthesized here is paired with graphite and Si-graphite anodes and successfully compensates for the first cycle IC, yielding better utilization of the cathode capacity in extended cycling.

Experimental

The $LiNi_{0.5}Mn_{1.5}O_4$ material used in this work was obtained from NEI corp. The liquid ammonia chemical lithiation was carried out using a lecture bottle station (Sigma-Aldrich). Approximately 30 mL of liquid ammonia was first condensed from an ammonia gas cylinder (anhydrous >99.99 %, Sigma-Aldrich) in a dry and argon purged round-bottom flask coupled with a cold finger condenser (Sigma-Aldrich). The condenser was kept cool by addition of dry ice to 2-propanol (Fisher Chemical). Reagents were added to the flask while maintaining a positive pressure of argon in the flask and exposure to the atmosphere was minimized. While stirring with a magnetic stirrer, 1 g of LNMO powder was added and allowed to disperse thoroughly in the ammonia. Small pieces of Li metal chips (MTI) were weighed and slowly added to the reaction vessel, allowing time for each chip to dissolve and react with the LNMO powder. The amount of lithium added controlled the amount of lithium inserted into the LNMO structure. The reaction took place over an approximately 6 h period, during which the reaction vessel was kept cool by

addition of dry ice to 2-propanol in a surrounding hemispherical Dewar (Sigma-Aldrich). Subsequently, the ammonia was allowed to evaporate by allowing the system to slowly increase in temperature. Without exposing the products to air, the reaction vessel was transferred to an argon filled glove box (O_2 and H_2O <1 ppm). The resulting powder was removed from the flask and washed in methanol (anhydrous ≥99.8 %, Sigma-Aldrich) until the pH of the solution was neutral. Collected lithiated LNMO powders (LLNMO) were dried at room temperature and stored in an argon glove box.

The cathodes in this work were prepared by casting a slurry of 84 wt.% active material (LNMO or LLNMO), 8 wt.% conductive carbon (Super P, Timcal), and 8 wt.% polyvinylidene fluoride binder (PVDF, Solvay) in N-methyl-2-pyrrolidone (NMP, ≥99.0 %, Sigma-Aldrich) solvent onto 20 μm thick Al foil. Slurry preparation and electrode casting were performed in an air atmosphere to test the air stability of the lithiated materials. Cathodes were dried under vacuum at 75 °C prior to use. Graphite anodes were prepared in a similar manner, with a ratio of 90 wt.% graphite (Hitachi MAGE), 2 wt.% conductive carbon (C45, Timcal), and 8 wt.% PVDF. Si-graphite composite electrodes were supplied by the Cell Analysis Modelling and Prototyping facility (CAMP), comprising of 73 wt.% graphite, 15 wt.% silicon (Nano-Amor, 50-70 nm), 2 wt.% conductive carbon (C45), and 10 wt.% lithiated polyacrylic acid binder (LiPAA, from 450k mol wt. PAA [Sigma-Aldrich] titrated against LiOH to pH 5.5-6.5). Graphite and Si-graphite electrodes were dried under vacuum at 120 °C and 150 °C, respectively, before use.

Electrodes with 1.43 cm diameter were punched and built into CR2032 coin cells (Hohsen) in both half- and full-cell configurations. Li chips (15.9 mm diameter, MTI) were used in half-cell tests. An electrolyte with 1.2 M $LiPF_6$ in ethylene carbonate (EC): ethyl methyl carbonate (EMC), 3:7 wt/wt (Tomiyama) was generally used. Cells containing a Si-graphite electrode used the above

electrolyte with additive 10 wt.% fluoroethylene carbonate (FEC, Solvay). Electrochemical cycling was conducted on a MACCOR series 4000 battery testing unit. Half-cells with LNMO or LLNMO were cycled between 4.95-3.5 V at C/10 (1C = 148 mAh g^{-1}_{LNMO}). Graphite and Si-graphite half-cells were cycled between 1.5-0.01 V and 1.5-0.05 V, respectively, at C/10 (graphite 1C = 350 mAh g^{-1}, Si-graphite 1C = 750 mAh $g^{-1}_{Si\text{-}graphite}$). Full cells were cycled at C/10 (1C = 148 mAh g^{-1} by cathode active mass, ~0.044 mA cm^{-2}) between 4.8-3.4 V at room temperature for graphite containing cells, and 4.8-3.45 V at 30 °C for Si-graphite cells. Cells were balanced by controlling the thickness of the electrode. The mass loading of the LNMO and LLNMO paired with graphite was ~2.0 mg cm^{-2}, and ~3.0 mg cm^{-2} when paired with Si-graphite. Graphite loading was ~1.1 mg cm^{-2} and Si-graphite loading was ~0.7 mg cm^{-2}.

The structure of the pristine and lithiated LNMO was confirmed by high-resolution synchrotron X-ray diffraction (XRD) at beamline 11-BM at the Advanced Photon Source (APS) at Argonne National Laboratory (Argonne, (λ = 0.41266 Å or 0.414534 Å)). Scanning electron microscope (SEM) images were captured using either a JEOL JSM6610LV microscope operated at 10 kV or a Hitachi S-4700-II microscope in the Electron Microscopy Center of Argonne. The Li, Ni and Mn molar ratio was analyzed using an Inductively Coupled Plasma – Mass Spectrometry (ICP-MS) DRCII; Perkin Elmer; Shelton, CT, USA. The LNMO or LLNMO powder was dissolved in concentrated HNO_3/HCl and diluted to the low ppb level for measurement. Rietveld refinements were performed using GSAS-II.[33]

Atomic-resolution imaging studies were performed on three cathode materials, $Li_{1.04}Ni_{0.5}Mn_{1.5}O_4$, $Li_{1.26}Ni_{0.5}Mn_{1.5}O_4$ and $Li_{1.62}Ni_{0.5}Mn_{1.5}O_4$. The scanning transmission electron microscopy (STEM) was carried out using an aberration-corrected JEOL ARM200CF, equipped with a cold field emission operated at 200 kV.[34] A convergence semi-angle of 24 mrad was used

and annular bright field (ABF) images[35-36] were acquired using an inner detector angle of 12 mrad and an outer angle of 24 mrad.[37] The TEM samples were prepared in a glove box under an argon environment to prevent any changes to the sample structure as the result of exposure to oxygen. The samples were loaded into a Fischione single-tilt vacuum transfer stage and exposure of the cathode samples to the ambient atmosphere was thereby minimized.

Results

Liquid ammonia chemical lithiation

Solutions of alkali metals in ammonia are widely used in synthetic organic chemistry to reduce aromatic compounds. Arthur Birch, an Australian chemist, first reported the "Birch reduction" reaction in 1944, in which sodium metal in ammonia was used to reduce benzene in the presence of ethanol.[38-43] Lithium, sodium, potassium, rubidium, cesium (alkali metals), calcium, strontium and barium (alkali earth metals) have all been shown to form solutions with ammonia.[44] The solution of lithium metal and ammonia is a deep blue color, consisting of an ammonia complexed lithium cation and a solvated electron ($[Li(NH_3)_x]^+ e^-$) known as an electride salt. This solution is a powerful reducing agent that, in contact with LNMO, will reduce Mn^{4+} to Mn^{3+}. To provide change compensation, lithium ions are inserted into the structure thereby lithiating the LNMO.

Firstly, the impact of the ammonia treatment on the crystal structure of LNMO was determined. The pristine material was stirred in ammonia for the same time as the lithiation experiments, but lithium metal was not added. XRD patterns of the pristine and ammonia treated LNMO are shown in Figure S1, and show no change from immersion in ammonia. To confirm lithium insertion into the LNMO spinel structure during the lithiation experiments XRD, ICP-MS

and electrochemical testing were performed. XRD patterns of the LNMO and lithiated LNMO (LLNMO) after washing with anhydrous methanol are shown in Figure 1. All the peaks in the XRD pattern of the pristine material, with lithium content $Li_{1.04}NMO$ as determined by ICP, can be assigned to a face-centered cubic phase with *Fd*-3*m* space group. With an increasing amount of lithium inserted there is an increase in intensity for reflections associated with the tetragonal $Li_2M_2O_4$ phase (in this case M = Ni, Mn, Figure 1),[45-46] most notably at 4.94, 9.12, 9.88, 10.84 and 11.69 ° 2θ (d spacing 4.79, 2.60, 2.40, 2.18, 2.03 Å). Rietveld analysis of the patterns (Figure S2) reveal constant lattice parameters for the cubic Li_1NMO and tetragonal Li_2NMO phases (a_c = 8.1829±0.0011 Å, a_t = 5.7306±0.0010 Å, c_t = 8.7281±0.0072 Å, where c and t represent cubic and tetragonal, respectively) with varying lithium content, indicative of a two-phase lithiation process. Refinement also shows that the weight fraction of the tetragonal Li_2NMO phase increases with lithium content (Table 1) at the expense of the cubic Li_1NMO phase.

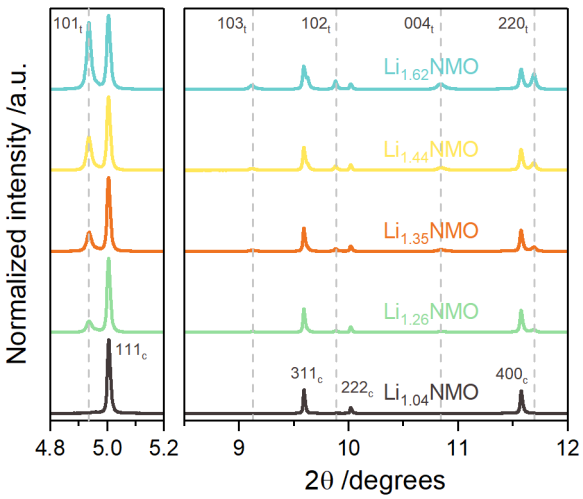

Figure 1: Normalized high-resolution synchrotron X-ray diffraction patterns of $LiNi_{0.5}Mn_{1.5}O_4$ and chemically lithiated $Li_{1+x}Ni_{0.5}Mn_{1.5}O_4$ (wavelength 0.412664 Å). Gray dashed lines denote the location of diffraction peaks of tetragonal $Li_2Ni_{0.5}Mn_{1.5}O_4$. Miller indices for the cubic (c) and tetragonal (t) phases are shown.

Table 1: Stoichiometry of $LiNi_{0.5}Mn_{1.5}O_4$ and chemically lithiated $Li_{1+x}Ni_{0.5}Mn_{1.5}O_4$.

Targeted stoichiometry	ICP stoichiometry			Calculated Mn fraction		Tetragonal spinel wt. fraction
	Li	Ni	Mn	Mn(III)	Mn(IV)	
$LiNi_{0.5}Mn_{1.5}O_4$	1.04(2)	0.480(1)	1.520(1)	0.05	0.95	-
$Li_{1.4}Ni_{0.5}Mn_{1.5}O_4$	1.26(3)	0.493(1)	1.507(2)	0.18	0.82	0.217(1)
$Li_{1.5}Ni_{0.5}Mn_{1.5}O_4$	1.35(2)	0.491(1)	1.509(1)	0.24	0.76	0.303(1)
$Li_{1.6}Ni_{0.5}Mn_{1.5}O_4$	1.44(3)	0.488(7)	1.512(7)	0.31	0.69	0.409(1)
$Li_{1.9}Ni_{0.5}Mn_{1.5}O_4$	1.62(1)	0.495(5)	1.504(5)	0.42	0.58	0.546(1)
$Li_{>2}Ni_{0.5}Mn_{1.5}O_4$	1.96(1)	0.515(5)	1.484(5)	0.64	0.36	

Lithiated samples that have not been washed with anhydrous methanol show the presence of a LiOH impurity in the high-resolution XRD pattern (Figure S3). Washing effectively removes this impurity. LiOH presence likely arises from the reaction of residual lithium amide ($LiNH_2$) formed during synthesis with trace levels of moisture in the glove box. A second observation from Figure S3 is a small change in the relative intensity of the tetragonal Li_2NMO 101 reflection compared to the cubic Li_1NMO 111 reflection at 4.94 and 5.01 ° 2θ, respectively. This indicates that anhydrous methanol washing has the effect of slightly delithiating the material, converting a small fraction of the lithium-rich tetragonal phase to the cubic phase. Given the importance of removing basic species (e.g., LiOH) from the powder to prevent electrode slurry processing problems (e.g., jelling) in NMP, this minor change is perhaps unavoidable. Alternative washing medium will be explored in future work.

Results from ICP-MS of the metal content in the pristine and lithiated samples are shown in Table 1, along with the targeted stoichiometry. Note that all references to the lithium content in LLNMO samples in this work are based on the *measured* ICP stoichiometry. In all cases, the measured lithium content is lower than that targeted. This is consistent with the finding that lithium salts are removed from the samples during washing. In fact, the measured lithium content tracks linearly with the targeted content, with a slope of 0.66(1) and y-intercept of 0.02(1) (Figure S4, $r^2 = 0.998$). Using this chemical lithiation method, the highest achieved lithium content is $Li_{1.96}$NMO.

Adding additional lithium to the reaction is ineffective at lithiating the material beyond this apparent Li_2NMO limit. Based on the ICP results, the fraction of Mn^{3+} and Mn^{4+} in the structure is calculated, assuming Ni^{2+} (Table 1). In $Li_{1.62}$NMO, the highest lithium content employed in this work, the fraction of Mn^{3+} is 42 %. This introduces Jahn-Teller distortion associated with high spin Mn^{3+} ($(t_{2g})^3 (e_g^*)^1$). Repeated formation of Mn^{3+} has been linked to structural degradation and rapid capacity fade in these materials,[47] and therefore it is best avoided. In this work, we minimize this effect by oxidizing the Mn^{3+} to Mn^{4+} on the first charge of the cell (delivering the extra lithium from the cathode to the anode) and then limiting the potential window to ensure Mn^{4+} is not reduced on discharge.

Electrochemical tests were also performed to verify the amount of electrochemically available lithium chemically inserted into the LLNMO. Upon charge, the pristine $Li_{1.04}$NMO exhibits a capacity of 145 mAh g^{-1} with plateaus at 4.71 and 4.76 V versus Li/Li^+ (Figure 2a). There is also a short sloping feature at ~4 V, which has been attributed to oxidation of a small amount of Mn^{3+} present.[48] As displayed in Figure 2a, the first charge capacity increases with the insertion of extra lithium. Extra lithium is mostly extracted in a sloping voltage feature at 3.8-4.0 V, although there is an additional feature at ~3.5 V and a plateau at 4.55 V that are absent in the $Li_{1.04}$NMO potential profile. These features are consistent with that observed previously for $Li_{1.8}$LNMO prepared by a microwave-assisted chemical lithiation process,[14] and are tentatively assigned to lithium extraction from different crystal environments that are sequentially emptied on charging. $Li_{1.62}$NMO shows a first charge capacity of 217 mAh g^{-1}. Therefore, XRD, ICP and electrochemistry all confirm that extra lithium has been inserted in the spinel structure of LNMO. Further, this extra lithium is electrochemically available; it can be extracted on the first charge and used to mitigate the first cycle irreversibility of the anode in full cells.

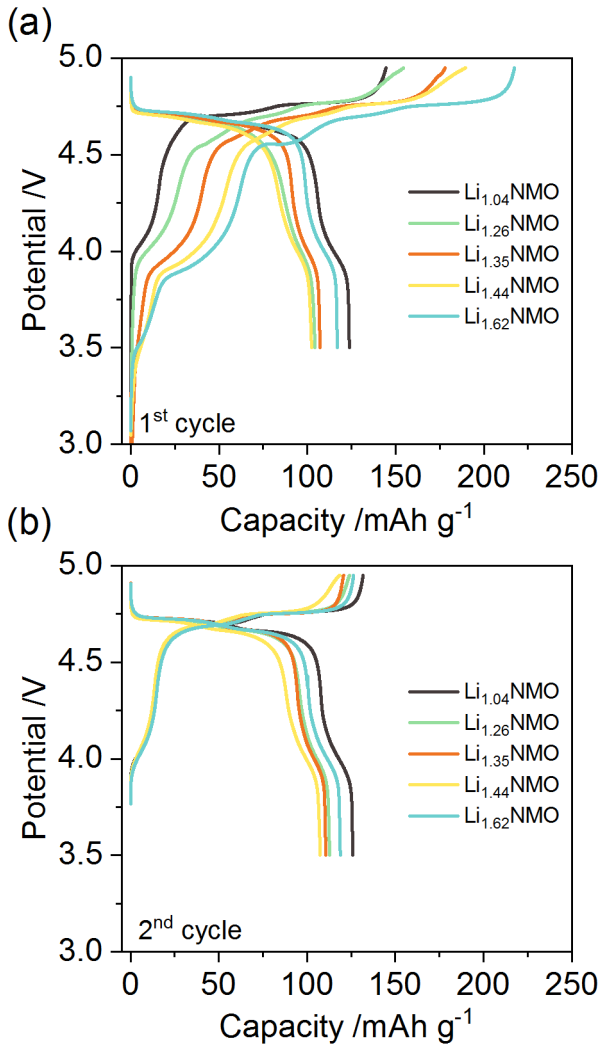

Figure 2: Potential profiles for the (a) first and (b) second charge and discharge of $LiNi_{0.5}Mn_{1.5}O_4$ and chemically lithiated $Li_{1+x}Ni_{0.5}Mn_{1.5}O_4$ versus lithium metal at a rate of C/10.

Before testing the performance of these lithiated cathode materials in full cells however, the reversibility and cycle stability of the LLNMO is compared with the baseline LNMO. Note that in the continued cycling a lower potential cut-off of 3.5 V is employed. In this manner, the structural distortion (from Mn^{3+} formation) is only endured a single time on the first charge. Thereafter LLNMO is cycled in a conventional potential window for LNMO (3.5-4.95 V, one Li^+ extraction/insertion per formula unit), which is anticipated to yield stable capacity retention comparable to pristine LNMO. Consideration of the potential profile on the first cycle (Figure 2a)

and in the second cycle (Figure 2b) highlights the relative reversibility of $Li_{1.04}NMO$ and LLNMO to a lower potential cut-off of 3.5 V versus Li/Li^+. In general, lithiated materials show a lower first discharge capacity ranging from 102-117 mAh g^{-1} compared to 124 mAh g^{-1} for $Li_{1.04}NMO$. This has also been observed for microwave-assisted chemical lithiation of LNMO,[14] and attributed to possible mechanical degradation of the active material during the lithation. In the current work, there is not a clear trend between the reversible capacity and the amount of extra lithium, suggesting the degree of lithiation is not the determining factor. Residual contamination in the LLNMO powder not removed by the washing process may detrimentally affect the reversibility. It is likely that material processing optimization will decrease the spread in reversibility of LLNMO. Other possible causes for the lower discharge capacity are discussed below in relation to changes in the particle morphology, as seen by SEM. The cycle stability of LNMO and LLNMO were tested at a C/10 rate to determine whether the presence of larger amounts of Mn^{3+} in the lithiated structure during the initial charge had a detrimental effect on capacity retention. This result is shown in Figure 3, and illustrates that while the discharge capacity is lower for LLNMO, over 40 cycles the stability of LLNMO is comparable with baseline LNMO.

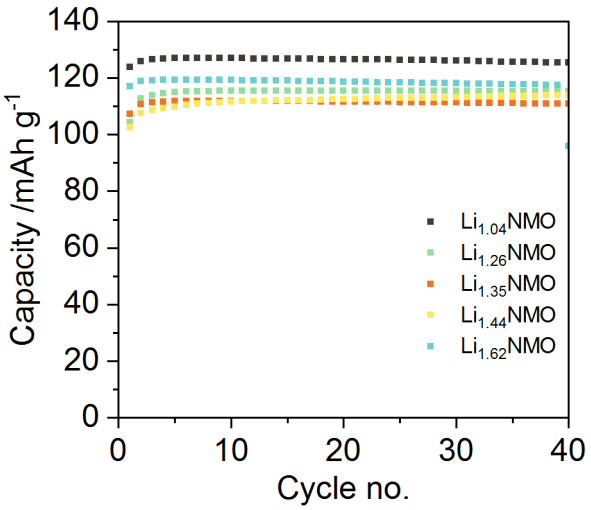

Figure 3: Discharge capacity over 40 cycles for $LiNi_{0.5}Mn_{1.5}O_4$ and chemically lithiated $Li_{1+x}Ni_{0.5}Mn_{1.5}O_4$ versus lithium metal at a rate of C/10.

To understand the effect of lithiation on the morphology of the LNMO particles, SEM images were taken before and after lithiation. While the overall particle size, popcorn-like shape and agglomeration generally remains unchanged, as Figures 4a-e and 4f–j reflect, severe particle cracking is found in some of the $Li_{1.44}$NMO and $Li_{1.62}$NMO particles (see Figures 4n and o). Evidently, the high concentration of Jahn-Teller active Mn^{3+} (31 % and 42 % of the total Mn in $Li_{1.44}$NMO and $Li_{1.62}$NMO, respectively) creates structural distortion and strain severe enough to generate cracks. At lower extents of lithiation the distortion is likely less and therefore it does not give rise to particle cracking (as displayed Figures 4k-m), since the grain boundaries possibly buffer the anisotropic expansion. Certainly, the particle degradation and loss of particle contact from cracking may give rise to a lower reversible capacity for LLNMO. Furthermore, the lower discharge capacity observed for LLNMO could be related to an irreversible structural change, in which the spinel structure after removal of the excess lithium is not equivalent to the pristine structure. It has been demonstrated that cycling spinels below 3 V leads to severe capacity fade,[47] a consequence of repeated formation of Mn^{3+} and the associated structural distortion. While in this work the distortion is only induced once, during synthesis, and alleviated on the first charge, it is still possible that the structural changes are detrimental to the reversible capacity of the material. It is worth noting that the stability of the lithiated materials are on par with the pristine material when cycled to a 3.5 V lower cut-off potential. In the work of Mancini et al.[30] LNMO with a more ideal particle architecture is synthesized, which appears to be capable of accommodating the strain and volume expansion during lithiation since no cracking is evident for their thermally synthesized Li_2NMO. It is surmised that optimizing the precursor LNMO for chemical lithiation processing is an important step, and will be the focus of further investigation. Finally, we note that the ammonia-

based lithiation method used in this work alters the particle architecture in some cases. Besides the presence of cracks at high lithiation levels of $Li_{1+x}Ni_{0.5}Mn_{1.5}O_4$ ($x \geq 0.44$), we have observed a well-defined laminated morphology in certain regions of $Li_{1.62}$NMO (see Figure S5). This could justify the slightly better electrochemical performance of $Li_{1.62}$NMO in contrast to the other LLNMO materials, since the presence of these planes may facilitate lithium (de)intercalation.

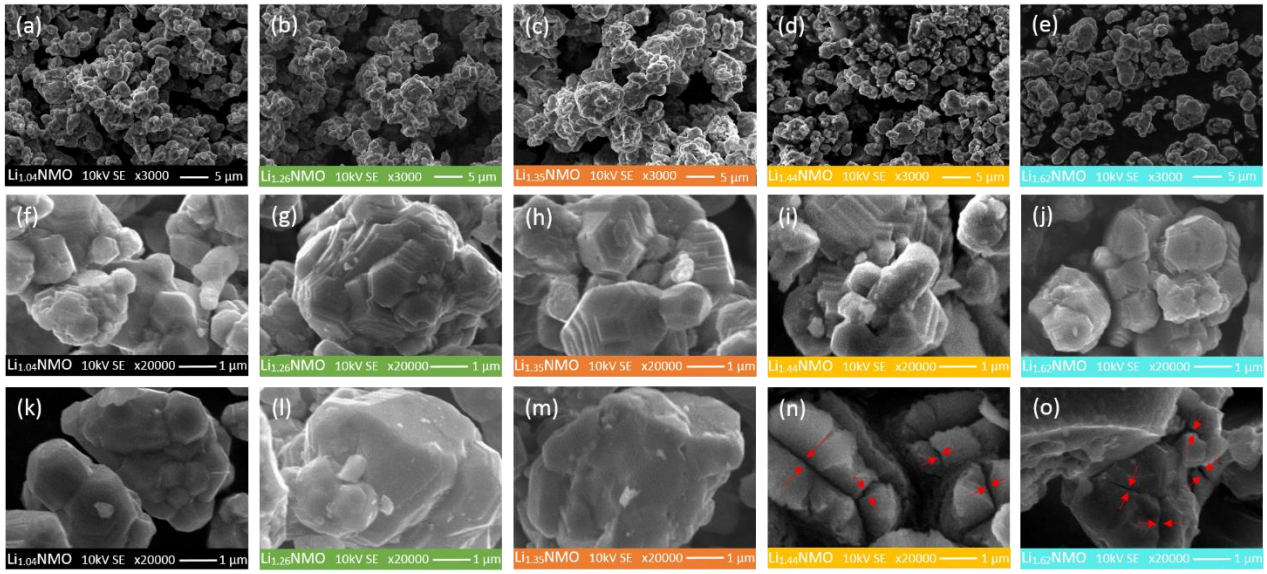

Figure 4: Scanning electron microscopy images of (a, f, k) $Li_{1.04}Ni_{0.5}Mn_{1.5}O_4$ and chemically lithiated (b, g, l) $Li_{1.26}Ni_{0.5}Mn_{1.5}O_4$, (c, h, m) $Li_{1.35}Ni_{0.5}Mn_{1.5}O_4$, (d, i, n) $Li_{1.44}Ni_{0.5}Mn_{1.5}O_4$ and (e, j, o) $Li_{1.62}Ni_{0.5}Mn_{1.5}O_4$ at magnification x3000 (top panels) and x20000 (center and bottom panels). Red arrows highlight the particle cracking present in high lithium content $Li_{1+x}Ni_{0.5}Mn_{1.5}O_4$.

STEM studies were performed to examine the atomic-scale structure of the pristine and lithiated materials. Particles from the pristine $Li_{1.04}$NMO powder (not shown here), exhibited the expected spinel structure.[49] The particles did not exhibit any notable surface layer in the pristine particles. Figure 5 shows a summary of the structural characterization of $Li_{1.62}$NMO. The atomic-resolution STEM ABF images (Figure 5b), which are sensitive to light elements such as Li and O, show a distinct core-shell structure. The core/bulk of the particles is identified as the $LiNi_{0.5}Mn_{1.5}O_4$ phase in the (001) projection. In this projection the Ni, Mn and O atomic column are aligned in the (001) direction to form a square lattice, while the Li atomic columns can be seen

as layers in every other (011) plane, as shown in Figure 5a. These Li planes can be directly seen in the ABF images and are indicted by the arrows in Figure 5b. The additional feature in the electron diffraction pattern for $LiNi_{0.5}Mn_{1.5}O_4$ due to the Li (0 ½ ½) is shown in Figure 5a.

The shell of the $Li_{1.62}$NMO particles exhibits a structure different from the bulk, where the layers of Li atoms are no longer visible. Detailed imaging and diffraction analysis reveals that the shell consists of a few nanometers of $Li_2Ni_{0.5}Mn_{1.5}O_4$ in the (100) projection. The atomic-structure and diffraction pattern are shown in Figure 5a, and a comparison with the STEM ABF images (Figure 5c) shows good agreement. It is interesting to note here that the $Li_2Ni_{0.5}Mn_{1.5}O_4$ surface layers form coherently on the particle surfaces. We did not find any defects or dislocations at the interface between the $LiNi_{0.5}Mn_{1.5}O_4$ core and the $Li_2Ni_{0.5}Mn_{1.5}O_4$ shell structures, suggesting that the mobility of Li diffusion should not be affected by the presence of this surface layer. Similar features are also observed in the $Li_{1.26}$NMO material.

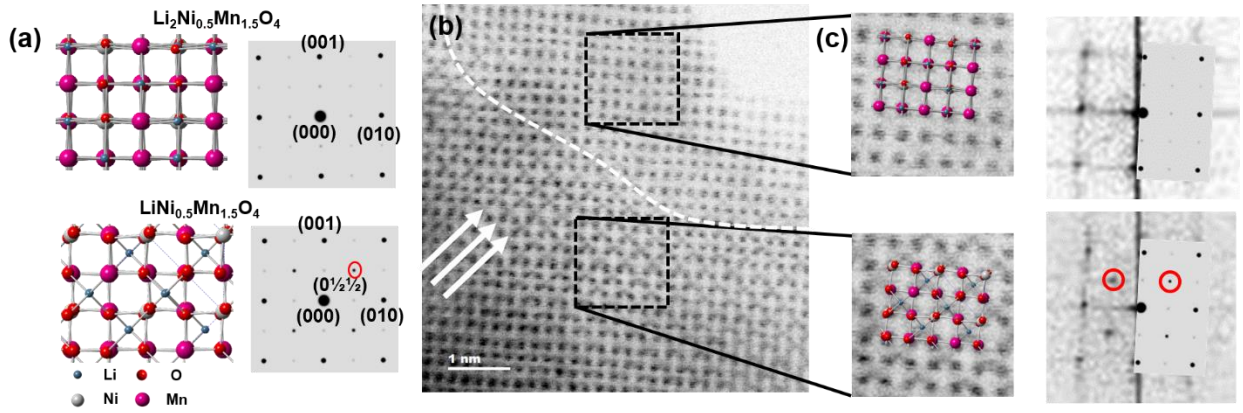

Figure 5: Electron microscopy analysis of $Li_{1.62}Ni_{0.5}Mn_{1.5}O_4$: a) ball-and-stick model of $Li_2Ni_{0.5}Mn_{1.5}O_4$ and $LiNi_{0.5}Mn_{1.5}O_4$ in the (100) orientation. The simulated electron diffraction patterns are also shown and the additional (0 ½ ½) reflection is highlighted in red for $LiNi_{0.5}Mn_{1.5}O_4$. b) Atomic-resolution annular bright field image of a $Li_{1.62}Ni_{0.5}Mn_{1.5}O_4$ particle showing a core shell structure. c) Magnified views of the particle shell showing a $Li_2Ni_{0.5}Mn_{1.5}O_4$ (100) structure, as confirmed by electron diffraction. A magnified view of the bulk structure ($LiNi_{0.5}Mn_{1.5}O_4$ (100)) is shown in the bottom part.

Full cell electrochemistry

The purpose of the chemical over-lithiation in this work is to provide additional lithium to the full cell to compensate for the first cycle IC of the anode. To test the effectiveness of the ammonia-based chemical lithiation method introduced, two anodes are selected. The first is graphite, the anode active material found in most commercial LIB, which has a relatively small first cycle IC (8.3 %). A Si-graphite composite electrode is the second anode considered, which has a larger first cycle IC (14.5 %). The IC of the graphite and Si-graphite electrodes were quantified by constructing half-cells and cycling them at C/10, as shown in Figure 6. Calculating the amount of capacity lost in the first cycle allowed us to match each anode with a LLNMO with an appropriate amount of extra lithiation capacity. In balancing the electrodes in a full cell, care was taken to ensure that the areal capacity ratio of negative to positive electrodes (n/p ratio)[50] never fell below 1.1. From these considerations, graphite was paired with $Li_{1.35}NMO$ and Si-graphite was paired with $Li_{1.62}NMO$. For comparison, baseline graphite//$Li_{1.04}NMO$ and Si-graphite//$Li_{1.04}NMO$ cells were also tested under the same conditions.

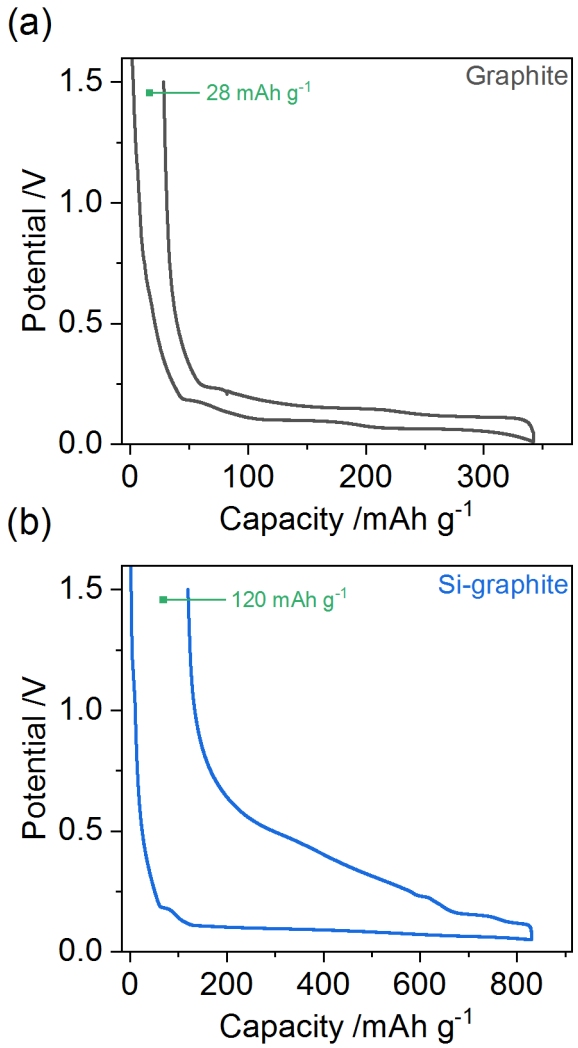

Figure 6: Potential profiles for the first cycle of (a) graphite and (b) Si-graphite versus lithium metal at a rate of C/10 highlighting the irreversible capacity in mAh g^{-1} of active material.

For simplicity in the following discussion, cells will be referred to by their point of difference, namely the cathode lithium content Li_xNMO. The first and second charge and discharge curves for the graphite containing full cells are shown in Figure 7. In the first charge, $Li_{1.35}NMO$ delivers 159 mAh g^{-1}_{LNMO} of capacity compared to 139 mAh g^{-1}_{LNMO} for $Li_{1.04}NMO$, a difference of 20 mAh g^{-1}_{LNMO}. Most of the extra capacity is extracted below 4.5 V. Upon discharge, $Li_{1.35}NMO$ shows a lower discharge capacity (102 mAh g^{-1}_{LNMO}) compared to $Li_{1.04}NMO$ (105 mAh g^{-1}_{LNMO}), however. This is consistent with the half-cell result for $Li_{1.35}NMO$, which showed

a reversible capacity 17 mAh g^{-1} lower than that of $Li_{1.04}NMO$ (107 mAh g^{-1} and 124 mAh g^{-1}, respectively). Because of this, both the baseline and pre-lithiated cells show similar discharge capacities in the first few cycles. Interestingly, from cycle 5 to 20, $Li_{1.35}NMO$ shows better capacity retention and higher Coulombic efficiency than $Li_{1.04}NMO$ (Figure 8). This is related to the pre-lithiation and the lower reversibility of $Li_{1.35}NMO$, which combined lead to a reserve of available lithium left on the anode at the end of the first discharge. The reserve of lithium is gradually diminished on a per cycle basis, with the rate of loss related to the extent of active lithium loss from cellular irreversible processes, such as SEI formation/repair. The "knee" present in the potential profile at ~3.8 V for $Li_{1.35}NMO$ but absent for $Li_{1.04}NMO$ (Figure 7) is also evidence for a lithium reserve in the former cells. This is explained in detail in the supplementary information with the aid of Figure S6, and relates to which electrode (cathode or anode) causes the full cell termination voltage to be reached. Beyond 20 cycles, the capacity of $Li_{1.35}NMO$ decreases to the same value as $Li_{1.04}NMO$ and then fades at the same rate. After 100 cycles, the discharge capacity and Coulombic efficiency are equivalent, within the error. This infers that there are no gains by using the LLNMO prepared in this work to compensate for the IC of graphite. Using a thermal lithiation synthesis for LLNMO, Gabrielli et al.[31] do observe a slight improvement in the capacity of graphite//LLNMO cells compared to graphite//LNMO cells. However, since the IC of graphite in their work is ~12 %, the capacity gain is minimal (~4 mAh g^{-1}_{LNMO} higher for the LLNMO electrode versus graphite compared to the as-prepared LNMO after 20 cycles).

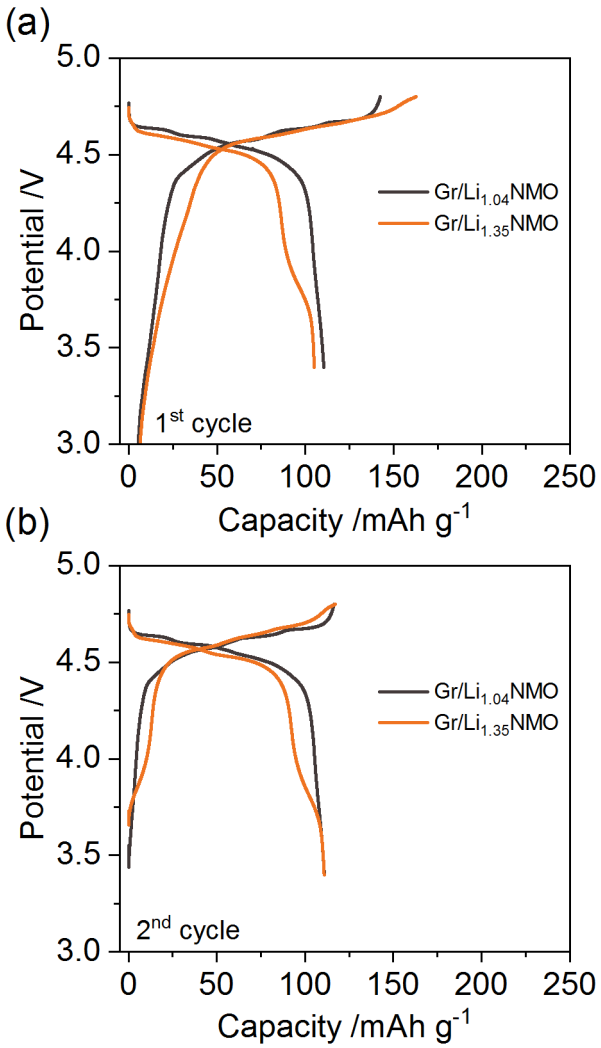

Figure 7: Full cell potential profiles for the (a) first and (b) second charge and discharge of $LiNi_{0.5}Mn_{1.5}O_4$ and chemically lithiated $Li_{1.35}Ni_{0.5}Mn_{1.5}O_4$ versus a graphite anode at a rate of C/10.

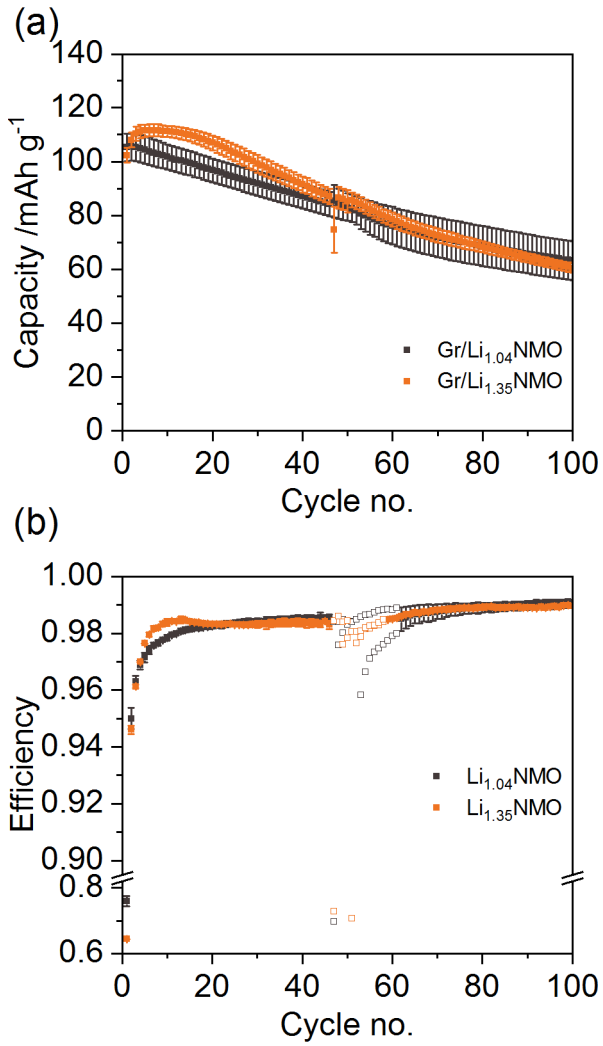

Figure 8: Full cell (a) discharge capacity and (b) cycle efficiency over 100 cycles for $LiNi_{0.5}Mn_{1.5}O_4$ and chemically lithiated $Li_{1.35}Ni_{0.5}Mn_{1.5}O_4$ versus graphite at a rate of C/10. Filled data symbols represent the average of two duplicate cells, with error bars showing the deviation between them. The open data symbols in (b) represent the region where a scheduled ~20 h power shutdown interrupted cycling and the subsequent cell recovery/break-in time (cycles 47-58 or 47-61). In this region data is shown from the two cells separately since they were interrupted on different cycle numbers.

Pre-lithiation becomes more important when the IC of the anode is large. To illustrate this, the first and second cycle potential profiles of Si-graphite//$Li_{1.04}$NMO and Si-graphite//$Li_{1.62}$NMO full cells are shown in Figure 9. Due to the larger IC of the Si-graphite electrode, the Coulombic efficiency for $Li_{1.04}$NMO is 57 % (charge and discharge capacity of 147 and 85 mAh g^{-1}_{LNMO}, respectively). Conversely, with pre-lithiation the first charge capacity of $Li_{1.62}$NMO is 201 mAh

g^{-1}_{LNMO}, with a reversible capacity of 104 mAh g^{-1}_{LNMO}. The reversible capacity is therefore 19 mAh g^{-1}_{LNMO} higher for the cells where the IC is compensated by the cathode pre-lithiation; a 23 % improvement. The increased first discharge capacity carries over into subsequent cycles (Figure 9b), and after 100 cycles at C/10 the cells with $Li_{1.62}NMO$ deliver 44 mAh g^{-1}_{LNMO} of capacity (Figure 10). This is 18 mAh g^{-1}_{LNMO} higher than the baseline $Li_{1.04}NMO$ case. Additionally, the capacity retention over 100 cycles is higher for $Li_{1.62}NMO$ relative to $Li_{1.04}NMO$ (42 % and 30 %, respectively).

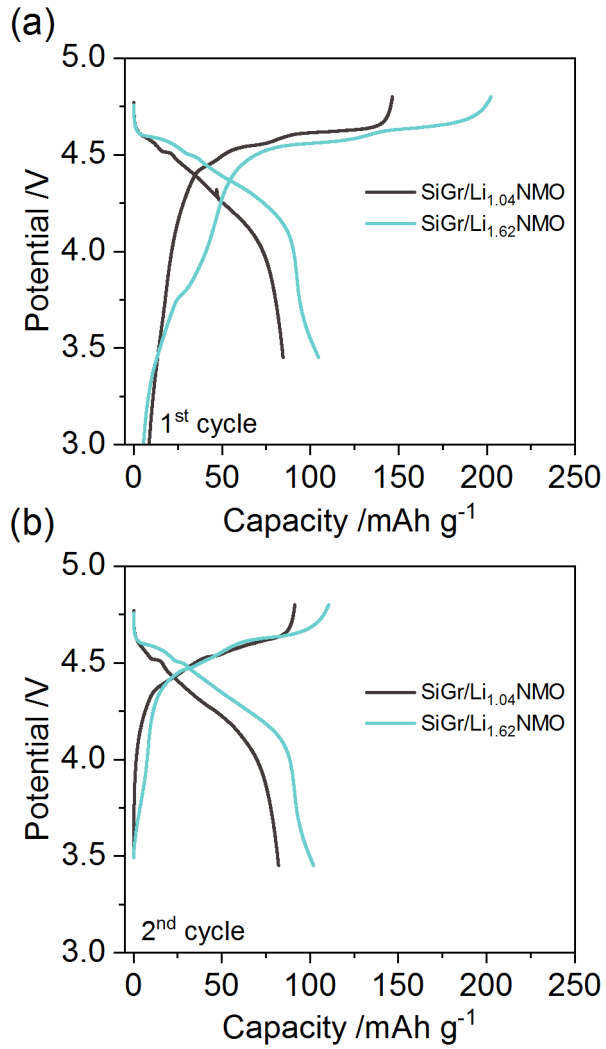

Figure 9: Full cell potential profiles for the (a) first and (b) second charge and discharge of $LiNi_{0.5}Mn_{1.5}O_4$ and chemically lithiated $Li_{1.62}Ni_{0.5}Mn_{1.5}O_4$ versus a Si-graphite composite anode at a rate of C/10.

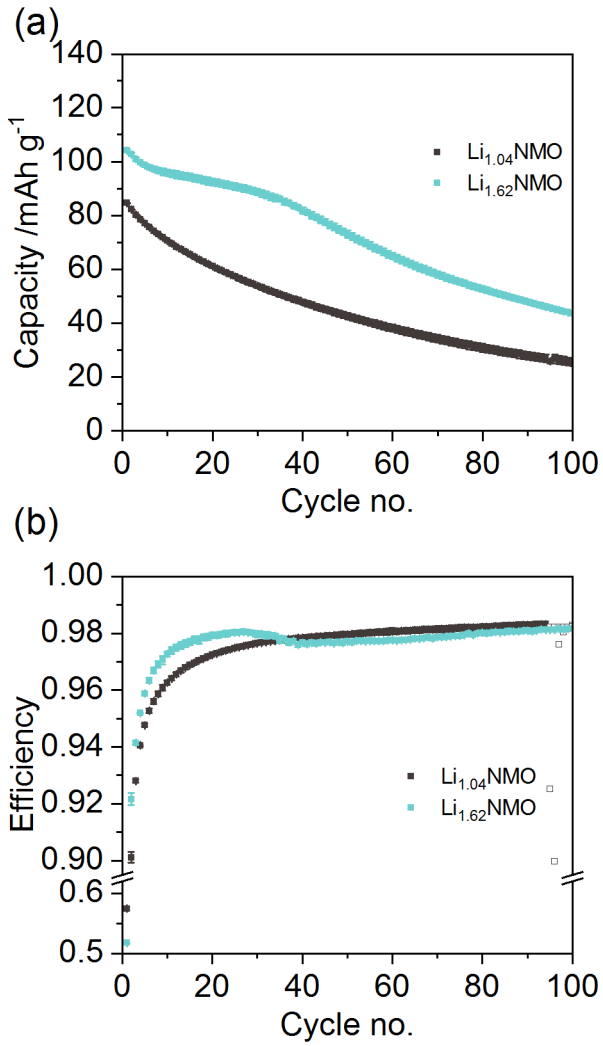

Figure 10: Full cell (a) discharge capacity and (b) cycle efficiency over 100 cycles for $LiNi_{0.5}Mn_{1.5}O_4$ and chemically lithiated $Li_{1.62}Ni_{0.5}Mn_{1.5}O_4$ versus Si-graphite at a rate of C/10. Filled data symbols represent the average of two duplicate cells, with error bars showing the deviation between them. The open data symbols in (b) represent the region where a scheduled ~20 h power shutdown interrupted cycling of $LiNi_{0.5}Mn_{1.5}O_4$ and the subsequent cell recovery/break-in time (cycles 95-100). In this region data is shown from the two cells separately since they were interrupted on different cycle numbers.

In Figure 9 and 10 there are clear signs that the Si-graphite anode in $Li_{1.62}$NMO cells has not been fully emptied after the first cycle, as was the case for graphite//$Li_{1.35}$NMO cells. As a result, a higher Coulombic efficiency and good capacity retention from cycle 2 to 34 are observed for $Li_{1.62}$NMO compared to $Li_{1.04}$NMO. The anode lithium reserve is apparently exhausted around cycle 34 and the Coulombic efficiency of $Li_{1.62}$NMO decreases to match that of $Li_{1.04}$NMO (97.8

% at cycle 35) and the capacity fade begins to track more closely. For example, between cycle 70 and 100 the capacity fade in cells with and without cathode pre-lithiation is equivalent, at 75 % retention over these 30 cycles. Moorhead-Rosenberg et al.[14] also observed higher cycling capacity but equivalent capacity fade rate with a FeSb-TiC anode paired against LNMO and LLNMO synthesized with microwave assisted chemical lithiation. Therefore, pre-lithiation does not generally alter the rate of active lithium loss in the full cell. One reported instance where pre-lithiation has had a secondary beneficial effect on the cycle life is in work from Gasteiger's group[51]. Lithium oxalate is used as a cathode additive with LNMO and paired with graphite and Si-graphite. During the first charge, the lithium salt is oxidized, releasing available lithium to the cell, which compensates for the first cycle IC. Concomitantly, carbon dioxide gas is released, which was shown in earlier work by Krause et al.[52] to be an effective SEI-forming additive, thereby improving the cycle life until the gas is consumed.

The equivalent fade rate noted between cathodes with and without pre-lithiation establishes that the pre-lithiation has had no detrimental effects on the cycling. However, in both the graphite and Si-graphite systems the rate of fade is substantially higher than desired. This highlights two issues that require further attention. The first is the capacity fade attributable to Mn dissolution.[53-55] This effect is the dominant cause for capacity fade in the graphite full cells, arising from Mn dissolution, migration and incorporation into the graphite SEI. Once there, Mn ions increase the rate of SEI growth, reducing solvent molecules and trapping lithium ions.[56-61] Much research has been dedicated to addressing this issue for the 4 V ($LiMn_2O_4$) and 5 V ($LiNi_{0.5}Mn_{1.5}O_4$) spinel materials, through surface coatings, bulk dopants, surface dopants, or more stable electrolyte and/or additive combinations (see ref.[62] for a recent review). For example, Zhang et al.[63-65] have reported a fluorinated electrolyte that demonstrates enhanced voltage stability in graphite/LNMO

cells cycled to 4.9 V and at 55 °C. Their results demonstrate improved capacity retention and higher Coulombic efficiency with less solid decomposition products on both electrodes.

The capacity retention with a Si-graphite anode is lower than with graphite (30 % compared to 60 %, respectively, over 100 cycles at C/10 against $Li_{1.04}$NMO), which highlights the second reason for capacity fade in this study. In addition to Mn dissolution problems, (de)lithiation of silicon during repeated cycling results in large volume expansion and contraction of the particles.[17] SEI delamination, reformation and repair is therefore continuously taking place each cycle, irreversibility and constantly depleting the active, cyclable lithium. Further, the repeated volume changes and increasing quantities of delaminated SEI products cause electrode degradation in the form of cracking, active particle isolation and electrode densification (loss of porosity).[18-19, 21] Therefore, while pre-lithiation provides a satisfactory solution to mitigate the first cycle IC, the capacity fade problems arising from Mn dissolution (at the cathode) and silicon cycling instability (at the anode) remain major research challenges.

Conclusions

Pre-lithiation of the cathode is achieved in this work by a novel and tunable liquid ammonia-based chemical lithiation synthesis method. The 5 V spinel cathode $LiNi_{0.5}Mn_{1.5}O_4$ was chemically lithiated by this method, with $Li_{1.96}Ni_{0.5}Mn_{1.5}O_4$ being the highest lithium composition achieved. Atomic-resolution STEM reveals the lithiated materials have a core-shell structure, with the $Li_2Ni_{0.5}Mn_{1.5}O_4$ phase forming coherent layers that are a few nanometers thick on the $LiNi_{0.5}Mn_{1.5}O_4$ bulk structure. Electrochemical tests confirm the chemically inserted lithium is electrochemically active and therefore suitable to compensate for the irreversible capacity in a full cell. Chemical pre-lithiation of the cathode appreciably improved the reversible capacity of full

cells with a Si-graphite anode. Importantly, the air stability of the lithiated cathode was sufficient to prepare electrodes in an air environment, with potential for improvement by using a dry atmosphere. The proposed ammonia-based chemical lithiation method demonstrated here for $LiNi_{0.5}Mn_{1.5}O_4$ may be extended to other lithium-ion battery cathode materials. The lithium inventory introduced by this technique compensates for irreversible, lithium consuming, processes in the cell, and has particular significance for next-generation high capacity anodes with a large irreversible capacity.

Acknowledgements

Support from the Vehicle Technologies Program, Hybrid and Electric Systems, in particular, David Howell, Tien Duong, Peter Faguy, and Brian Cunningham at the U.S. Department of Energy (DOE), Office of Energy Efficiency and Renewable Energy is gratefully acknowledged. This manuscript has been created by UChicago Argonne, LLC, Operator of Argonne National Laboratory (a DOE Office of Science laboratory) under Contract No. DE-AC02-06CH11357. This research used resources of the Advanced Photon Source, a U.S. Department of Energy (DOE) Office of Science User Facility operated for the DOE Office of Science by Argonne National Laboratory under Contract No. DE-AC02-06CH11357. This work was performed, in part, at the Center for Nanoscale Materials, a U.S. Department of Energy Office of Science User Facility under Contract No. DE-AC02-06CH11357. The authors acknowledge Dean Bass for assistance obtaining the ICP-MS data, and Cameron Peebles for assistance collecting the SEM images. XR and RFK acknowledge funding from the National Science Foundation (DMR-1831406) to support the STEM imaging study. Use of the JEOL JEM-ARM200CF in the Electron

Microscopy Core of UIC's Research Resource Center was supported by two grants from the National Science Foundation (DMR-0959470 and DMR-1626065).

For Table of Contents Only

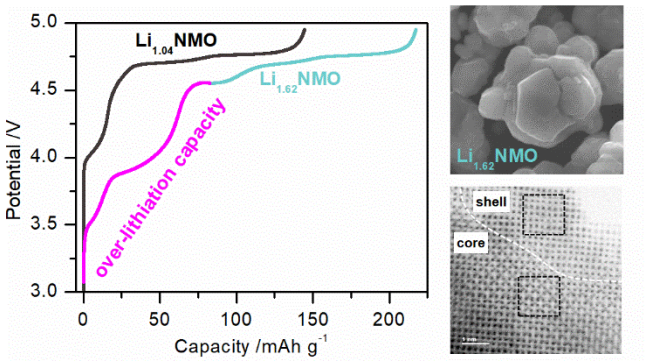

References

1. Thackeray, M. M.; Wolverton, C.; Isaacs, E. D., Electrical energy storage for transportation—approaching the limits of, and going beyond, lithium-ion batteries. *Energy & Environmental Science* **2012,** *5* (7), 7854-7863.
2. Yoo, H. D.; Markevich, E.; Salitra, G.; Sharon, D.; Aurbach, D., On the challenge of developing advanced technologies for electrochemical energy storage and conversion. *Materials Today* **2014,** *17* (3), 110-121.
3. Poizot, P.; Laruelle, S.; Grugeon, S.; Dupont, L.; Tarascon, J. M., Nano-sized transition-metal oxides as negative-electrode materials for lithium-ion batteries. *Nature* **2000,** *407*, 496.
4. Hu, Y.-Y.; Liu, Z.; Nam, K.-W.; Borkiewicz, O. J.; Cheng, J.; Hua, X.; Dunstan, M. T.; Yu, X.; Wiaderek, K. M.; Du, L.-S.; Chapman, K. W.; Chupas, P. J.; Yang, X.-Q.; Grey, C. P., Origin of additional capacities in metal oxide lithium-ion battery electrodes. *Nature Materials* **2013,** *12*, 1130.
5. Obrovac, M. N.; Chevrier, V. L., Alloy Negative Electrodes for Li-Ion Batteries. *Chemical Reviews* **2014,** *114* (23), 11444-11502.
6. Su, X.; Wu, Q.; Li, J.; Xiao, X.; Lott, A.; Lu, W.; Sheldon, B. W.; Wu, J., Silicon-Based Nanomaterials for Lithium-Ion Batteries: A Review. *Advanced Energy Materials* **2013,** *4* (1), 1300882.
7. Courtney, I. A.; Dahn, J. R., Electrochemical and In Situ X-Ray Diffraction Studies of the Reaction of Lithium with Tin Oxide Composites. *Journal of The Electrochemical Society* **1997,** *144* (6), 2045-2052.
8. Winter, M.; Besenhard, J. O., Electrochemical lithiation of tin and tin-based intermetallics and composites. *Electrochimica Acta* **1999,** *45* (1), 31-50.
9. Chan, C. K.; Zhang, X. F.; Cui, Y., High Capacity Li Ion Battery Anodes Using Ge Nanowires. *Nano Letters* **2008,** *8* (1), 307-309.

10. Xu, K., Electrolytes and Interphases in Li-Ion Batteries and Beyond. *Chemical Reviews* **2014,** *114* (23), 11503-11618.
11. Xu, K., Nonaqueous Liquid Electrolytes for Lithium-Based Rechargeable Batteries. *Chemical Reviews* **2004,** *104* (10), 4303-4418.
12. Cheng, X.-B.; Zhang, R.; Zhao, C.-Z.; Wei, F.; Zhang, J.-G.; Zhang, Q., A Review of Solid Electrolyte Interphases on Lithium Metal Anode. *Advanced Science* **2015,** *3* (3), 1500213.
13. Verma, P.; Maire, P.; Novák, P., A review of the features and analyses of the solid electrolyte interphase in Li-ion batteries. *Electrochimica Acta* **2010,** *55* (22), 6332-6341.
14. Moorhead-Rosenberg, Z.; Allcorn, E.; Manthiram, A., In Situ Mitigation of First-Cycle Anode Irreversibility in a New Spinel/FeSb Lithium-Ion Cell Enabled via a Microwave-Assisted Chemical Lithiation Process. *Chemistry of Materials* **2014,** *26* (20), 5905-5913.
15. Aravindan, V.; Lee, Y.-S.; Madhavi, S., Best Practices for Mitigating Irreversible Capacity Loss of Negative Electrodes in Li-Ion Batteries. *Advanced Energy Materials* **2017,** *7* (17), 1602607.
16. Holtstiege, F.; Wilken, A.; Winter, M.; Placke, T., Running out of lithium? A route to differentiate between capacity losses and active lithium losses in lithium-ion batteries. *Physical Chemistry Chemical Physics* **2017,** *19* (38), 25905-25918.
17. Beaulieu, L. Y.; Eberman, K. W.; Turner, R. L.; Krause, L. J.; Dahn, J. R., Colossal Reversible Volume Changes in Lithium Alloys. *Electrochemical and Solid-State Letters* **2001,** *4* (9), A137-A140.
18. Michan, A. L.; Divitini, G.; Pell, A. J.; Leskes, M.; Ducati, C.; Grey, C. P., Solid Electrolyte Interphase Growth and Capacity Loss in Silicon Electrodes. *Journal of the American Chemical Society* **2016,** *138* (25), 7918-7931.
19. Radvanyi, E.; Porcher, W.; De Vito, E.; Montani, A.; Franger, S.; Jouanneau Si Larbi, S., Failure mechanisms of nano-silicon anodes upon cycling: an electrode porosity evolution model. *Physical Chemistry Chemical Physics* **2014,** *16* (32), 17142-17153.
20. Wetjen, M.; Solchenbach, S.; Pritzl, D.; Hou, J.; Tileli, V.; Gasteiger, H. A., Morphological Changes of Silicon Nanoparticles and the Influence of Cutoff Potentials in Silicon-Graphite Electrodes. *Journal of The Electrochemical Society* **2018,** *165* (7), A1503-A1514.
21. Oumellal, Y.; Delpuech, N.; Mazouzi, D.; Dupré, N.; Gaubicher, J.; Moreau, P.; Soudan, P.; Lestriez, B.; Guyomard, D., The failure mechanism of nano-sized Si-based negative electrodes for lithium ion batteries. *Journal of Materials Chemistry* **2011,** *21* (17), 6201-6208.
22. Yoon, T.; Nguyen, C. C.; Seo, D. M.; Lucht, B. L., Capacity Fading Mechanisms of Silicon Nanoparticle Negative Electrodes for Lithium Ion Batteries. *Journal of The Electrochemical Society* **2015,** *162* (12), A2325-A2330.
23. Dose, W. M.; Maroni, V. A.; Piernas-Muñoz, M. J.; Trask, S. E.; Bloom, I.; Johnson, C. S., Assessment of Li-Inventory in Cycled Si-Graphite Anodes Using LiFePO4 as a Diagnostic Cathode. *Journal of The Electrochemical Society* **2018,** *165* (10), A2389-A2396.
24. Manthiram, A.; Chemelewski, K.; Lee, E.-S., A perspective on the high-voltage $LiMn_{1.5}Ni_{0.5}O_4$ spinel cathode for lithium-ion batteries. *Energy & Environmental Science* **2014,** *7* (4), 1339-1350.
25. U.S. Department of Energy, Secretary of Energy Rick Perry Announces $68.5 Million for Advanced Vehicle Technologies Research [Press Release], Retrieved from https://www.energy.gov/articles/secretary-energy-rick-perry-announces-685-million-advanced-vehicle-technologies-research. **2018, May 1**.

26. Ariyoshi, K.; Iwakoshi, Y.; Nakayama, N.; Ohzuku, T., Topotactic Two-Phase Reactions of $Li[Ni_{1/2}Mn_{3/2}]O_4$ (P4332) in Nonaqueous Lithium Cells. *Journal of The Electrochemical Society* **2004,** *151* (2), A296-A303.
27. Lee, E.-S.; Huq, A.; Chang, H.-Y.; Manthiram, A., High-Voltage, High-Energy Layered-Spinel Composite Cathodes with Superior Cycle Life for Lithium-Ion Batteries. *Chemistry of Materials* **2012,** *24* (3), 600-612.
28. Park, S.-H.; Oh, S.-W.; Yoon, C.-S.; Myung, S.-T.; Sun, Y.-K., $LiNi_{0.5}Mn_{1.5}O_4$ Showing Reversible Phase Transition on 3 V Region. *Electrochemical and Solid-State Letters* **2005,** *8* (3), A163-A167.
29. Park, S. H.; Oh, S. W.; Kang, S. H.; Belharouak, I.; Amine, K.; Sun, Y. K., Comparative study of different crystallographic structure of $LiNi_{0.5}Mn_{1.5}O_{4-\delta}$ cathodes with wide operation voltage (2.0–5.0V). *Electrochimica Acta* **2007,** *52* (25), 7226-7230.
30. Mancini, M.; Axmann, P.; Gabrielli, G.; Kinyanjui, M.; Kaiser, U.; Wohlfahrt-Mehrens, M., A High-Voltage and High-Capacity $Li_{1+x}Ni_{0.5}Mn_{1.5}O_4$ Cathode Material: From Synthesis to Full Lithium-Ion Cells. *ChemSusChem* **2016,** *9* (14), 1843-1849.
31. Gabrielli, G.; Marinaro, M.; Mancini, M.; Axmann, P.; Wohlfahrt-Mehrens, M., A new approach for compensating the irreversible capacity loss of high-energy Si/C|$LiNi_{0.5}Mn_{1.5}O_4$ lithium-ion batteries. *Journal of Power Sources* **2017,** *351*, 35-44.
32. Mancini, M.; Gabrielli, G.; Axmann, P.; Wohlfahrt-Mehrens, M., Electrochemical Performance and Phase Transitions between 1.5 and 4.9 V of Highly-Ordered $LiNi_{0.5}Mn_{1.5}O_4$ with Tailored Morphology: Influence of the Lithiation Method. *Journal of The Electrochemical Society* **2017,** *164* (1), A6229-A6235.
33. Toby, B. H.; Von Dreele, R. B., GSAS-II: the genesis of a modern open-source all purpose crystallography software package. *Journal of Applied Crystallography* **2013,** *46* (2), 544-549.
34. Klie, R. F.; Gulec, A.; Guo, Z.; Paulauskas, T.; Qiao, Q.; Tao, R.; Wang, C.; Low, K. B.; Nicholls, A. W.; Phillips, P. J., The new JEOL JEM-ARM200CF at the University of Illinois at Chicago. *Crystal Research and Technology* **2014,** *49* (9), 653-662.
35. Findlay, S. D.; Shibata, N.; Sawada, H.; Okunishi, E.; Kondo, Y.; Ikuhara, Y., Dynamics of annular bright field imaging in scanning transmission electron microscopy. *Ultramicroscopy* **2010,** *110* (7), 903-923.
36. Findlay, S. D.; Shibata, N.; Sawada, H.; Okunishi, E.; Kondo, Y.; Yamamoto, T.; Ikuhara, Y., Robust atomic resolution imaging of light elements using scanning transmission electron microscopy. *Applied Physics Letters* **2009,** *95* (19), 191913.
37. Phillips, P. J.; Klie, R. F., On the visibility of very thin specimens in annular bright field scanning transmission electron microscopy. *Applied Physics Letters* **2013,** *103* (3), 033119.
38. Birch, A. J., 117. Reduction by dissolving metals. Part I. *Journal of the Chemical Society (Resumed)* **1944,** (0), 430-436.
39. Birch, A. J., 212. Reduction by dissolving metals. Part II. *Journal of the Chemical Society (Resumed)* **1945,** (0), 809-813.
40. Birch, A. J., 119. Reduction by dissolving metals. Part III. *Journal of the Chemical Society (Resumed)* **1946,** (0), 593-597.
41. Birch, A. J., 25. Reduction by dissolving metals. Part IV. *Journal of the Chemical Society (Resumed)* **1947,** (0), 102-105.
42. Birch, A. J., 327. Reduction by dissolving metals. Part V. *Journal of the Chemical Society (Resumed)* **1947,** (0), 1642-1648.

43. Birch, A. J.; Mukherji, S. M., 532. Reduction by dissolving metals. Part VI. Some applications in synthesis. *Journal of the Chemical Society (Resumed)* **1949,** (0), 2531-2536.
44. Johnson, W. C.; Meyer, A. W., The Properties of Solutions of Metals in Liquid Ammonia. *Chemical Reviews* **1931,** *8* (2), 273-301.
45. Thackeray, M. M.; David, W. I. F.; Bruce, P. G.; Goodenough, J. B., Lithium insertion into manganese spinels. *Materials Research Bulletin* **1983,** *18* (4), 461-472.
46. David, W. I. F.; Thackeray, M. M.; De Picciotto, L. A.; Goodenough, J. B., Structure refinement of the spinel-related phases $Li_2Mn_2O_4$ and $Li_{0.2}Mn_2O_4$. *Journal of Solid State Chemistry* **1987,** *67* (2), 316-323.
47. Sun, Y.-K.; Jeon, Y.-S., Overcoming Jahn–Teller distortion of oxysulfide spinel materials for lithium secondary batteries. *Journal of Materials Chemistry* **1999,** *9* (12), 3147-3150.
48. Zhong, Q.; Bonakdarpour, A.; Zhang, M.; Gao, Y.; Dahn, J. R., Synthesis and Electrochemistry of $LiNi_xMn_{2-x}O_4$. *Journal of The Electrochemical Society* **1997,** *144* (1), 205-213.
49. Hayashi, K.; Okamoto, R.; Suzuki, N.; Matsumoto, S.; Terauchi, M.; Tsuda, K., Direct observation of Mn and Ni ordering in LiMn1.5Ni0.5O4 using atomic resolution scanning transmission electron microscopy. *Microscopy* **2018,** *67* (5), 280-285.
50. Kasnatscheew, J.; Placke, T.; Streipert, B.; Rothermel, S.; Wagner, R.; Meister, P.; Laskovic, I. C.; Winter, M., A Tutorial into Practical Capacity and Mass Balancing of Lithium Ion Batteries. *Journal of The Electrochemical Society* **2017,** *164* (12), A2479-A2486.
51. Solchenbach, S.; Wetjen, M.; Pritzl, D.; Schwenke, K. U.; Gasteiger, H. A., Lithium Oxalate as Capacity and Cycle-Life Enhancer in LNMO/Graphite and LNMO/SiG Full Cells. *Journal of The Electrochemical Society* **2018,** *165* (3), A512-A524.
52. Krause, L. J.; Chevrier, V. L.; Jensen, L. D.; Brandt, T., The Effect of Carbon Dioxide on the Cycle Life and Electrolyte Stability of Li-Ion Full Cells Containing Silicon Alloy. *Journal of The Electrochemical Society* **2017,** *164* (12), A2527-A2533.
53. Jang, D. H.; Shin, Y. J.; Oh, S. M., Dissolution of Spinel Oxides and Capacity Losses in 4 V $Li/Li_xMn_2O_4$ Cells. *Journal of The Electrochemical Society* **1996,** *143* (7), 2204-2211.
54. Delacourt, C.; Kwong, A.; Liu, X.; Qiao, R.; Yang, W. L.; Lu, P.; Harris, S. J.; Srinivasan, V., Effect of Manganese Contamination on the Solid-Electrolyte-Interphase Properties in Li-Ion Batteries. *Journal of The Electrochemical Society* **2013,** *160* (8), A1099-A1107.
55. MahootcheianAsl, N.; Kim, J.-H.; Pieczonka, N. P. W.; Liu, Z.; Kim, Y., Multilayer electrolyte cell: A new tool for identifying electrochemical performances of high voltage cathode materials. *Electrochemistry Communications* **2013,** *32*, 1-4.
56. Ochida, M.; Domi, Y.; Doi, T.; Tsubouchi, S.; Nakagawa, H.; Yamanaka, T.; Abe, T.; Ogumi, Z., Influence of Manganese Dissolution on the Degradation of Surface Films on Edge Plane Graphite Negative-Electrodes in Lithium-Ion Batteries. *Journal of The Electrochemical Society* **2012,** *159* (7), A961-A966.
57. Shin, H.; Park, J.; Sastry, A. M.; Lu, W., Degradation of the solid electrolyte interphase induced by the deposition of manganese ions. *Journal of Power Sources* **2015,** *284*, 416-427.
58. Gowda, S. R.; Gallagher, K. G.; Croy, J. R.; Bettge, M.; Thackeray, M. M.; Balasubramanian, M., Oxidation state of cross-over manganese species on the graphite electrode of lithium-ion cells. *Physical Chemistry Chemical Physics* **2014,** *16* (15), 6898-6902.
59. Zhan, C.; Lu, J.; Jeremy Kropf, A.; Wu, T.; Jansen, A. N.; Sun, Y.-K.; Qiu, X.; Amine, K., Mn(II) deposition on anodes and its effects on capacity fade in spinel lithium manganate–carbon systems. *Nature Communications* **2013,** *4*, 2437.

60. Shkrob, I. A.; Kropf, A. J.; Marin, T. W.; Li, Y.; Poluektov, O. G.; Niklas, J.; Abraham, D. P., Manganese in Graphite Anode and Capacity Fade in Li Ion Batteries. *The Journal of Physical Chemistry C* **2014,** *118* (42), 24335-24348.
61. Gilbert, J. A.; Shkrob, I. A.; Abraham, D. P., Transition Metal Dissolution, Ion Migration, Electrocatalytic Reduction and Capacity Loss in Lithium-Ion Full Cells. *Journal of The Electrochemical Society* **2017,** *164* (2), A389-A399.
62. Zhan, C.; Wu, T.; Lu, J.; Amine, K., Dissolution, migration, and deposition of transition metal ions in Li-ion batteries exemplified by Mn-based cathodes – a critical review. *Energy & Environmental Science* **2018,** *11* (2), 243-257.
63. Hu, L.; Zhang, Z.; Amine, K., Fluorinated electrolytes for Li-ion battery: An FEC-based electrolyte for high voltage $LiNi_{0.5}Mn_{1.5}O_4$/graphite couple. *Electrochemistry Communications* **2013,** *35*, 76-79.
64. Zhang, Z.; Hu, L.; Wu, H.; Weng, W.; Koh, M.; Redfern, P. C.; Curtiss, L. A.; Amine, K., Fluorinated electrolytes for 5 V lithium-ion battery chemistry. *Energy & Environmental Science* **2013,** *6* (6), 1806-1810.
65. Hu, L.; Xue, Z.; Amine, K.; Zhang, Z., Fluorinated Electrolytes for 5 V Li-Ion Chemistry: Synthesis and Evaluation of an Additive for High-Voltage $LiNi_{0.5}Mn_{1.5}O_4$/Graphite Cell. *Journal of The Electrochemical Society* **2014,** *161* (12), A1777-A1781.